Supplementary Information

Anchoring Side Chains to Carbonate Groups for Reviving Stable Polycarbonate-Based Solid-State Lithium Metal Batteries

Hantao Xu[1,2#], Wei Deng[1#], Jingyuan Yu[1#], Lei Shi[1], Wenwei Zhang[1], Juncai Long[1], Chaobin He[2,6*], Lin Xu[1,3,4,5*]

Affiliations

[1]State Key Laboratory of Advanced Technology for Materials Synthesis and Processing, School of Materials Science and Engineering, Wuhan University of Technology, Wuhan 430070 Hubei, P.R. China

[2]Department of Materials Science & Engineering, National University of Singapore, 9 Engineering Drive 1, Singapore, 117574 Singapore

[3]Hubei Longzhong Laboratory, Wuhan University of Technology (Xiangyang Demonstration Zone), Xiangyang 441000, Hubei, P. R. China

[4]Hainan Institute, Wuhan University of Technology, Sanya 572000, P. R. China

[5]Zhongyu Feima New Material Technology Innovation Center (Zhengzhou) Co., Ltd., High Technology Industrial Development Zone, Zhengzhou 450001, P. R. China

[6]Institute of Materials Research and Engineering, Agency for Science, Technology and Research, (A*STAR), Singapore, 138634 Singapore

Contributions

[#]Hantao Xu, Wei Deng and Jingyuan Yu contributed equally to this work.

Corresponding author

Correspondence to: msehc@nus.edu.sg; linxu@whut.edu.cn

Materials

2,2,2-Trifluoroethylamine, AIBN (recrystallization), acetone, trimethylamine (TEA), 2-isocyanatoethylmethacrylate, dimethyl ether (anhydrous, DME), sodium hydroxide, hydrochloric acid, sodium chloride, N-methyl-2-pyrrolidone (anhydrous, NMP) and dimethyl sulfoxide-d6 were purchased from Aladdin Co. Ltd. Anhydrous ethanol, dichloromethane, dimethyl sulfoxide (DMSO), tetrahydrofuran (THF), N,N-dimethylformamide (DMF) and anhydrous ether were purchased from Sinopharm Chemical Reagent Co. Ltd. Li metal anodes (ø14 × 0.6), 100 μm Li foils and 50 μm Li/Cu composite foils were purchased from China Energy Lithium Co., Ltd. Vinylene carbonate (VC, battery grade) and LiTFSI (battery grade) were purchased from Duoduo Reagent Co., Ltd. Porous PE separator was purchased from Chongqing Yuntianhua Co., Ltd. (China). All battery parts were purchased from Shenzhen Yongxing Precision Machinery Co., Ltd. Copper foils, NCM811, LFP microparticles and super P were purchased from MTI-KJ group (Shenzhen) and used after drying in the oven at 120 °C for 12 h. PVDF (5130) was purchased from Guangdong Canrd New Energy Technology Co., Ltd. The above all the chemicals were used directly as purchased without further purification treatment.

Synthesis of 2-(3-(2,2,2-trifluoroethyl)ureido)ethyl methacrylate (TUEM)

4.95 g 2,2,2-Trifluoroethylamine, 0.05 mL triethylamine, and 120 mL of dichloromethane were added to a 250 mL three-neck flask equipped with a magnetic stir bar and nitrogen purge at an ice water bath. Then, 7.75 g 2-isocyanatoethylmethacrylate was added dropwise to the mixture and stirred overnight at 0 °C. After the reaction was quenched by deionized water, the precipitated white solid (11.0 g) was filtered out by vacuum filtration and washed three times with cold dichloromethane. ^{1}H NMR and ^{19}F NMR can be seen in **Figure S1**. ^{1}H NMR (500 MHz, DMSO-d_6) δ 6.59 (t, J = 6.6 Hz, 1H), 6.30 (t, J = 6.0 Hz, 1H), 6.06 (s, 1H), 5.68 (t, J = 1.8 Hz, 1H), 4.08 (t, J = 5.5 Hz, 2H), 3.81 (qd, J = 9.8, 6.4 Hz, 2H), 3.33 (d, J = 4.4 Hz, 2H), 1.89 (s, 3H). ^{19}F NMR (471 MHz, DMSO-d_6) δ -71.76 (t, J = 9.7 Hz).

Preparation of P(TUEM-VC)-SPE (PTV-SPE)

The copolymer electrolyte of PTV-SPE was synthesized and prepared in an argon atmosphere glovebox. First, 0.25 g TUEM and 0.29 g LiTFSI were dissolved in 1.36 g (1 mL) of VC to give a homogeneous solution. Then, 1×10^{-2} mol L^{-1} AIBN was added to the solution. Next, 30 μL of the resulting solution was injected into 2016 lithium batteries, wherein a PE membrane was

adopted as the supporting matrix to separate the cathodes and Li metal anodes. These batteries were then kept at 55 °C for 6 h to obtain solid state PTV-SPE.

For the characterization of precipitated products, the polymer electrolytes were dissolved and collected by DMF, and the collected mixture was added to 100 mL ether and stirred for 6 h. The washed precipitate was washed 3 times with ether, and dried at 80 °C under vacuum, to give PTV as a white solid. ^{1}H NMR and ^{19}F NMR of PTV can be seen in **Figure 1c, Figure S3a**.

Preparation of PVC-SPE

In an argon atmosphere glovebox, 0.29 g LiTFSI were dissolved in 1 mL of VC to give a homogeneous and transparent solution. Then, 1×10^{-2} mol L^{-1} AIBN was added to the solution. Next, 30 μL of the resulting solution was injected into 2016 lithium batteries, wherein a PE membrane was adopted as the supporting matrix to separate the cathodes and Li metal anodes. These batteries were then kept at 55 °C for 6 h to obtain solid state PVC-SPE.

Calculations and simulations

All calculations were conducted using the Vienna Ab initio Simulation Package (VASP) and Materials Studio 2020 (MS)[1-3]. The Perdew-Burke-Ernzerhof (PBE) exchange-correlation functional[4], along with the DFT-D3 correction for van der Waals interactions[5], was employed to ensure accurate energy calculations. Initially, the bulk Li structure was optimized using the Conjugate Gradient (CG) method. The convergence criteria were set to 0.03 eV/Å for atomic forces and 10^{-5} eV for energy. Upon achieving structural optimization, the (100) surface of Li was cleaved to create a slab model suitable for molecular adsorption studies. The slab consisted of a 4 × 4 supercell of the Li (100) surface with a thickness of four atomic layers, ensuring an adequate representation of the surface properties. To prevent interactions between periodic images, a vacuum layer of 15 Å was included above the slab. For k-point sampling, the Monkhorst-Pack method was employed, utilizing a 3 × 3 × 1 grid to provide sufficient sampling of the Brillouin zone for the surface structure. To further investigate the dynamics of molecular adsorption and decomposition on the Li metal surface, ab initio molecular dynamics (AIMD) simulations were performed. The relevant figure was manually drawn based on actual calculated data. The simulations employed the Nosé thermostat to maintain the temperature at 300 K[6], with a time step set to 1 fs. All atoms were allowed to move freely during the simulation, thereby accurately capturing the molecular interactions and dynamics at the surface. Visualization of the computed

structures and molecular dynamics trajectories was performed using VESTA software[7], which facilitated detailed graphical representations of the atomic configurations and interactions.

The adsorption energy (E_{ad}) is a crucial parameter for quantifying the stability of molecules on a surface. It is defined as the energy difference between the total energy of the adsorbate-surface system and the energies of the isolated components. The adsorption energy can be calculated using the following equation:

$$E_{ad}=E_{total}-(E_{surface}+E_{adsorbate})$$

Where E_{total} is the total energy of the adsorbate-surface system, $E_{surface}$ and $E_{adsorbate}$ are the energies of the clean surface (before adsorption) and the isolated adsorbate, respectively. A negative value of E_{ad} indicates that the adsorption process is exothermic and that the adsorbate is more stable when bound to the surface, while a positive value suggests that adsorption is endothermic.

The charge density difference ($\Delta\rho$) is a valuable tool for analyzing the electronic interactions between an adsorbate and a surface. It is defined as the difference between the charge density of the adsorbate-surface system and the sum of the charge densities of the isolated components. The charge density difference can be expressed mathematically as:

$$\Delta\rho=\rho_{total}-(\rho_{surface}+\rho_{adsorbate})$$

Where ρ_{total} is the charge density of the combined adsorbate-surface system, $\rho_{surface}$ and $\rho_{adsorbate}$ are the charge density of the clean surface and the charge density of the isolated adsorbate. A positive value of $\Delta\rho$ indicates an increase in charge density in the region of interaction, suggesting charge accumulation, while a negative value implies charge depletion.

The MD simulations were performed by the Forcite module with COMPASS Ⅱ force field in MS[8-9]. Two solution systems were respectively constructed into cubic simulation boxes. The PVC/LiTFSI system contained 8 PVC molecules and 10 LiTFSI. The PTV/LiTFSI system consisted of the same number of PTV and LiTFSI molecules as PVC/LiTFSI system. Van der Waals and Coulomb interactions were respectively considered by atom based and Ewald methods with a cut-off value of 12.5 Å. Equations of motion were integrated with a time step of 1 fs. After energy minimization, each system was fully relaxed under periodic boundary conditions for 400 ps in the NPT (P = 1 atmosphere, T = 333.15 K) ensemble using the Nose thermostat and

Berendsen barostat, which was long enough for system temperature, potential and total energy to get stable. After reaching equilibrium state, another 400 ps simulation under NVT ensemble was performed to extract trajectory and data. The dynamic trajectory for each system was outputted at 4 ps interval and used for RDF and coordinate number calculation. The coordination number N_i of molecules i in the first solvation shell surrounding Li^+ was calculated as:

$$N_i = 4\pi\rho\int_0^{R_M} g(r)r^2dr$$

Where R_M is the distance of the first minimum following the first peak in the RDF $g(r)$ and ρ is the number density of molecules i[10].

Material characterization

X-ray diffraction (XRD) patterns were recorded using a Bruker D2 Advance with Cu Kα radiation. Solid-state NMR spectra of ^{6}Li NMR were measured in a double resonance 2.5 mm magic angle spinning probe with the relaxation delay of 10 s and rotation speed of 15 kHz on a Bruker Avance 400 MHz spectrometer. The structures of polymer electrolyte membranes before and after cycles were characterized through nuclear magnetic resonance (NMR) (Bruker 500 MHz spectrometer, ^{1}H, ^{19}F, ^{1}H-^{1}H COSY, ^{1}H-^{1}H NOESY in DMSO-d_6) (The impurity peak at ~1.1 and ~4.5 ppm is ethanol, ~2.7 and ~2.8 ppm is DMF, 3.3 ppm is water, 2.5 ppm is DMSO), temperature-dependent Fourier transform infrared spectrometers (FT-IR, Thermo Nicolet Corporation; 7800-350/cm 0.01/cm/6700). Nano-CT 3D reconstruction was measured in a phase mode for 18 hours scan on a Zeiss Xradia 810 Ultra. In situ ATR-FTIR measurements were conducted using a Thermo scientific iS50 spectrometer to test the chemical stability of 10 μL electrolytes towards lithium metal within simulated cells. Additionally, in situ ATR-FTIR measurements were conducted using a Linglu Battery Instruments cell equipped with a Pike ATR optical bench. The current density applied during testing was 0.1 mA cm^{-2}. The spectra were collected in external reflection using a liquid-N_2-cooled MCT (mercury−cadmium−telluride) detector, each pattern was acquired at each 100 s. The morphology of the cycled surface of lithium metal anodes (SEI) and polymer electrolyte membranes were examined via a ZEISS GeminiSEM 300 scanning electron microscope with an accelerating voltage of 2 kV. The X-ray photoelectron spectroscopy (XPS, ESCALAB 250 Xi spectrometer) analyses were used to measure the surface composition of the SEIs on the surface of lithium metal anodes, while the samples were rinsed with DME to remove impurities and electrolyte components from the SEI surface, and protected

in a glove box filled with Ar gas. The testing of molecular weight involved first dissolving the polymer electrolyte in DMF, and then precipitating it in ether before testing the GPC. GPC was recorded by an Agilent 1200 series HPLC with an MZ-GPC column and DMF was used as the elution solvent with a flow rate of 1.0 mL min^{-1}. TOF-SIMS measurements were conducted with a PHI nano TOF Ⅲ. A Bi_3^{++} beam (30 kV, 2 nA) with raster size of 100 μm was used as the primary beam to detect the samples, sputtering with an Cs^+ beam (2 kV, 100 nA, 400*400 μm^2), and the pre-treatment process of the sample is similar to that of XPS. The thermal stability was executed by thermogravimetric analysis (TGA) using a NETZSCH STA 449F5 instrument over the temperature range between 30 and 600 °C under Ar condition at a heating rate of 10 °C min^{-1}. A tensile testing machine (Shimadzu AGS-X-50N) was used to obtain the stress-strain curves with the tensile speed of 0.2 cm min^{-1}.

Ionic conductivity and activation energy

The stainless steel SS/electrolyte/SS cells were assembled to measure ionic conductivities. The electrochemical impedance spectroscopy (EIS) was measured in the temperature range from 30 °C to 70 °C (record every 10 °C) using an BioLogic EC-Lab VMP3 in the frequency range from 10^6 Hz to 10^2 Hz with a perturbation of 10 mV. The electrolytes were sandwiched between two pieces of stainless-steel blocking electrode with a diameter of 15.8 mm. and the ionic conductivity(σ)was calculated from the Equation:

$$\sigma = \frac{L}{R_b S}$$

Where L is the thickness of the electrolyte, S is the contact area between the two stainless steel plates, and R(Ω) is the bulk resistance of the electrolyte.

Electrochemical stability window

The electrochemical stability window and the electrochemical floating analysis of electrolytes can be measured by building Li/electrolyte/SS and Li/electrolyte/NCM cells and conducting linear sweep voltammetry (LSV) measurements range from 0−6 V at 1 mV s^{-1} via BioLogic EC-Lab VMP3.

Li^+ transference numbers

Li^+ Transference Number can be tested using Li/electrolyte/Li symmetric cells via BioLogic EC-Lab VMP3. The cell resistances are determined before and after polarization using EIS and currents measured by the DC method. $t_{Li}{}^+$ is obtained according to the following Equation:

$$t_{Li+} = \frac{I_s(\Delta V - I_0 R_0)}{I_0(\Delta V - I_s R_s)}$$

Where I_0 and I_s are the initial and steady-state currents. The R_0 and R_s are the resistances before and after polarization of the cell, respectively. ΔV is the DC potential applied across the cell.

Battery assembly and testing

Li/electrolyte/Li symmetric cells assembled using 100 μm Li foil in an argon-filled glovebox (H_2O < 0.01 ppm, O_2 < 0.01 ppm) were tested by a multichannel battery testing system (Land CT2001A, Wuhan Land Electronic Co. Ltd., China). A certain constant current density was applied to the battery and the current signal was changed every 60 minutes at room temperature. The depth of discharge (DOD) of the Li/Li symmetric cells were 2.4%. In situ electrochemical impedance spectroscopy (EIS) characterizations of symmetric Li/Li cells were assembled for evaluating the interfacial impedance change before and after electrochemical cycling using a BioLogic VMP3 multichannel electrochemical workstation. The distribution of relaxation times (DRT) was obtained using the MATLAB-GUI toolbox.[11] Tafel plots were acquired from cyclic voltammetry (CV) tests in Li/Li cells with a scan rate of 1.0 mV s^{-1}. The selected voltage ranges from 80 to 100 mV in the linear region were employed to calculate exchange current density (i_0). Coulombic efficiencies of Li plating and stripping cycles were studied in a Cu/Li cell configuration. The self-discharge performance, rate and cycle performance of cells were performed by using $LiNi_{0.8}Co_{0.1}Mn_{0.1}O_2$/electrolyte/Li and $LiFePO_4$/electrolyte/Li coin cells assembled in an argon-filled glovebox. The $LiNi_{0.8}Co_{0.1}Mn_{0.1}O_2$ and $LiFePO_4$ cathode slurry were prepared by commercially available cathode powder, Super P, and PVDF powder with a mass fraction of 8:1:1. The mass loading of cathodes were 2 mg cm^{-2}. The obtained cathode slurry was doctor-bladed on aluminum foils and then dried at 120 °C for 12 h in a vacuum oven. Then, the cathode foil was punched into a small plate with a diameter of 10 mm. Punching of 100 μm Li foil into a small plate with a diameter of 14 mm to be used as the anode of the full cell. C rates in $LiFePO_4$/electrolyte/Li cells were defined based on 1C=170 mAh g^{-1}. And The C rates in

$LiNi_{0.8}Co_{0.1}Mn_{0.1}O_2$/electrolyte/Li cells were defined based on 1C=200 mAh g^{-1}. The as-prepared $LiFePO_4$/electrolyte/Li cells then subjected to test its charging/discharging cyclic performance by charging to 4 V and discharging to 2.5 V on LAND testing system, and $LiNi_{0.8}Co_{0.1}Mn_{0.1}O_2$/Li cells test its charging/discharging cyclic performance by charging to 4.3 V/4.5 V and discharging to 2.7 V/3.0 V at room temperature on LAND testing system. The solid-state NCM811/Li (0.8 Ah, double-sided 10 mg cm^{-2} cathodes, 50 μm Li/Cu composite foils) pouch cell was assembled in an argon-filled glovebox (H_2O < 0.01 ppm, O_2 < 0.01 ppm) with PE separator and 3.5 mL precursors. After the first vacuum packaging of the pouch cell, it was heated to 50 °C for 12 h for in situ polymerization and high-temperature formation, then sat aside at room temperature for 24 h for room-temperature formation. The pouch cell (charging and discharging range: 3−4.25 V) was second vacuum sealed after the first formation cycle at 0.05 C and the second formation cycle at 0.1 C, and then it was charged/discharged at a constant current of 0.5 C at room temperature on NEWARE CT-4008-5V6A battery test system.

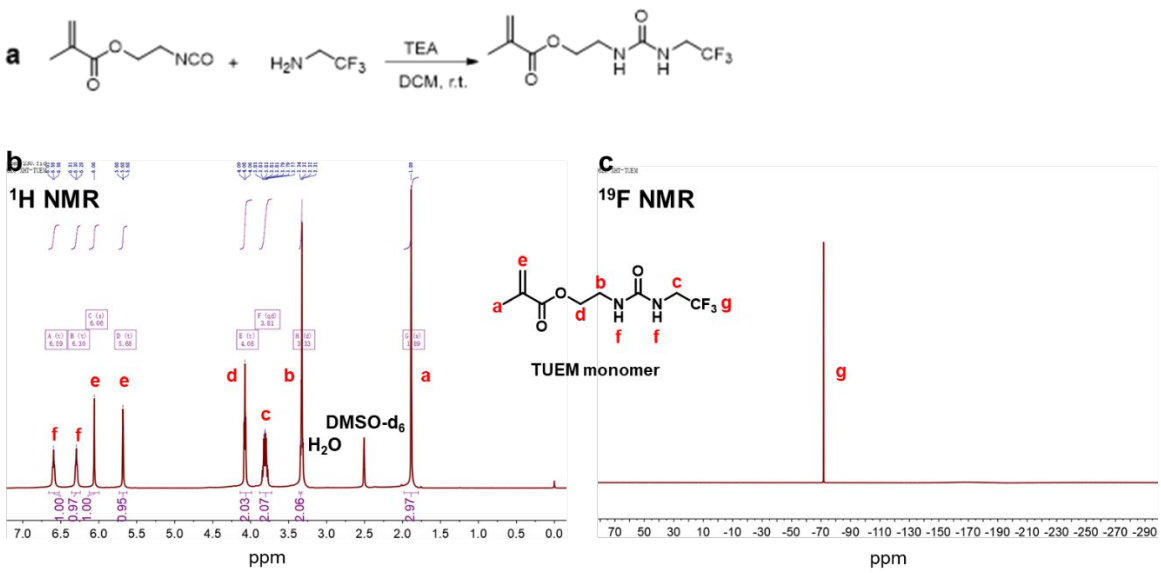

Figure S1. (a) The synthesis route of TUEM. (b) ^{1}H NMR spectrum of TUEM. (c) ^{19}F NMR spectrum of TUEM.

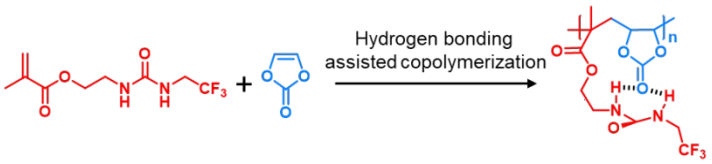

Figure S2. Schematic diagram of PTV copolymerization.

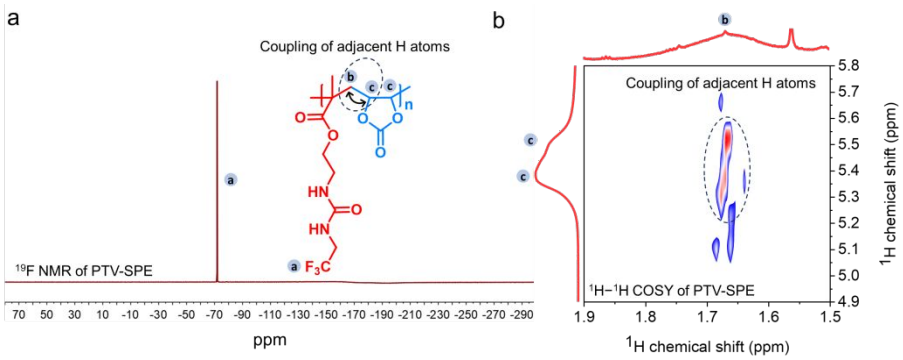

Figure S3. (a) ^{19}F NMR spectrum of PTV. (b) ^{1}H−^{1}H COSY experiment of PTV.

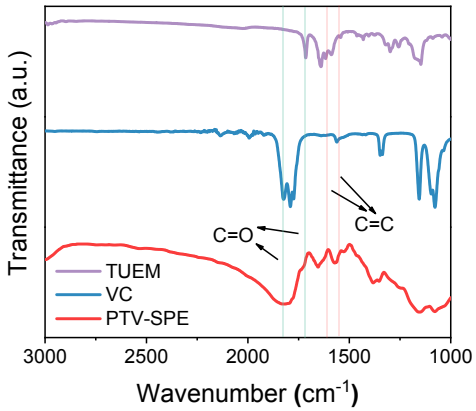

Figure S4. FT-IR spectra of PTV-SPE, VC monomer and TUEM monomer.

After polymerization, the C=C peaks located at 1618 cm^{-1} of TUEM and 1565 cm^{-1} of VC disappear. The C=O of VC located at 1831 cm^{-1} and the C=O of TUEM located at 1715 cm^{-1} remain in the same position.

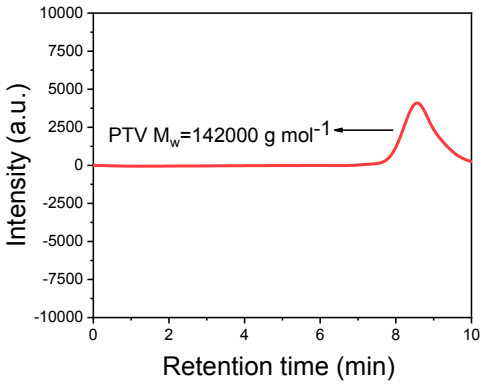

Figure S5. GPC curve of PTV-SPE.

GPC curve has only one peak, indicating that there is only one polymer product, which is a copolymer.

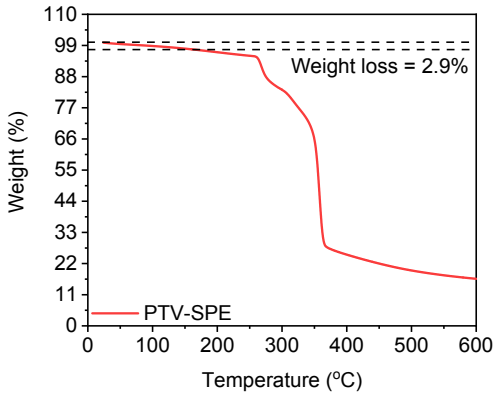

Figure S6. Thermogravimetric curve of PTV-SPE.

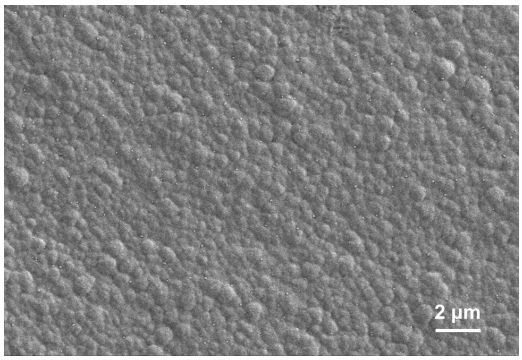

Figure S7. Top-view SEM image of PTV-SPE membrane.

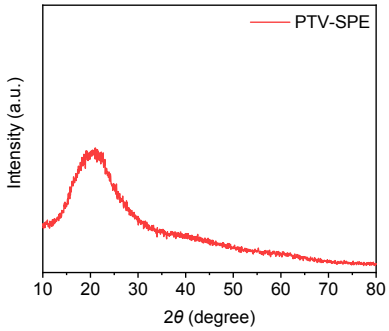

Figure S8. The XRD pattern of PTV-SPE.

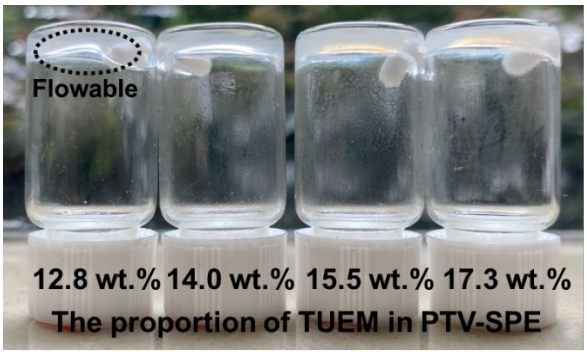

Figure S9. Photographs of PTV-SPE with varied mass fraction of TUEM.

As shown in **Figure S9**, the polymer electrolytes with copolymerized TUEM mass fractions above 15.5 wt.% show transparent solid states without any flowable liquid.

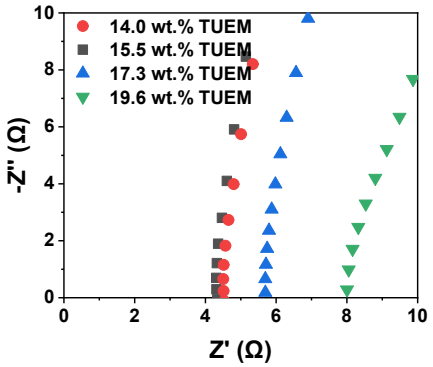

Figure S10. Impedance plots of different copolymerized TUEM mass fractions of PTV-SPE.

From **Figure S10**, it can be seen that within the solid-state range of **Figure S9**, the lowest bulk impedance of PTV-SPE is exhibited when the mass fraction of TUEM is 15.5 wt.%.

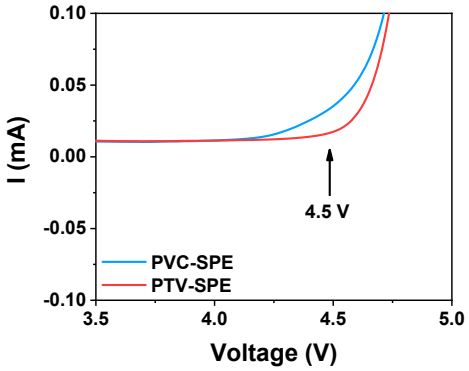

Figure S11. LSV curves of PTV-SPE and PVC-SPE.

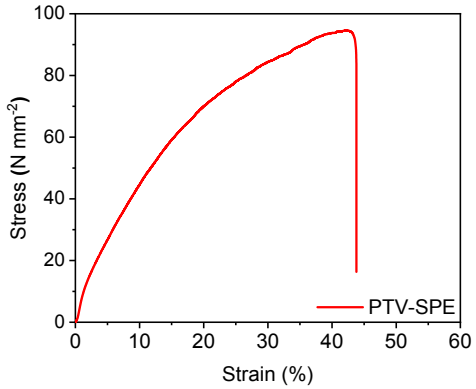

Figure S12. The stress-strain curve of PTV-SPE.

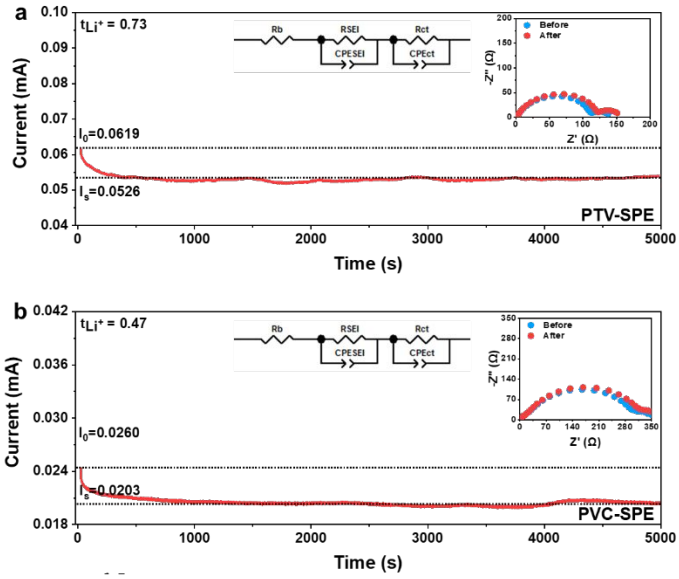

Figure S13. (a) The corresponding current-time profile following a DC polarization of 0.01 V for the Li/PTV-SPE/Li symmetrical cell at room temperature; Nyquist profiles of PTV-SPE of electrochemical impedance spectroscopy before and after polarization. (b) The corresponding current-time profile following a DC polarization of 0.01 V for the Li/PVC-SPE/Li symmetrical cell at room temperature; Nyquist profiles of PVC-SPE of electrochemical impedance spectroscopy before and after polarization.

The time-current curve of the Li/PTV-SPE/Li symmetric cell following a direct current (DC) polarization of 0.01 V for 5000 s at 25 °C is presented in **Figure S13**a. As we can see, the initial current is 0.0619 mA and then stabilizes at 0.0526 mA after polarization, and the corresponding interfacial impedance increases from 113.7 Ω to 124.8 Ω (**Figure S13**a). As a result, the PTV-SPE presents a t_{Li}^{+} of 0.73. In contrast, the time-current curve of the Li/PVC-SPE/Li symmetric cell following a DC polarization of 0.01 V at 25 °C is presented in **Figure S13**b. The initial current is 0.0260 mA and then stabilizes at 0.0203 mA after polarization, and the corresponding interfacial impedance increases from 304.5 Ω to 323.6 Ω (**Figure S13**b). The calculated t_{Li}^{+} of PVC-SPE is 0.47. The high t_{Li}^{+} of PTV-SPE reduces internal polarization by inhibiting the formation of concentration gradient.

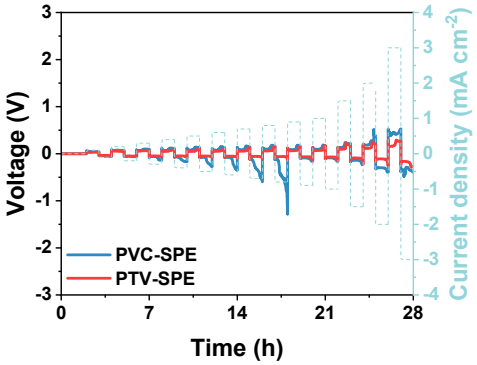

Figure S14. Voltage profiles of Li/Li symmetric cells with PTV-SPE and PVC-SPE at various current densities.

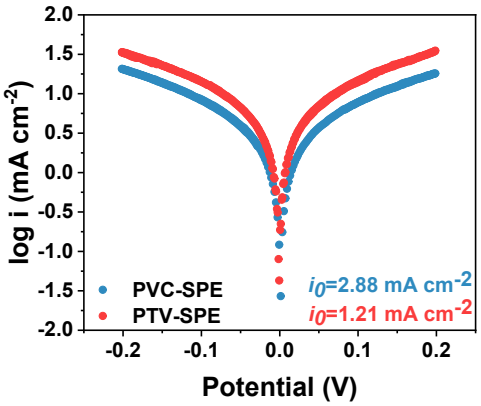

Figure S15. Tafel plots of PTV-SPE-based cell and PVC-SPE-based cell, and the corresponding exchange current densities are shown.

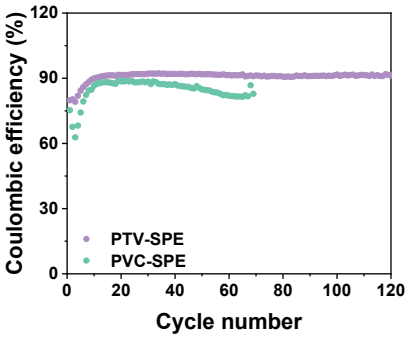

Figure S16. Coulombic efficiencies of Li plating/stripping in Cu/Li cells using PTV-SPE and PVC-SPE at 0.5 mA cm^{-2} and 0.5 mAh cm^{-2}.

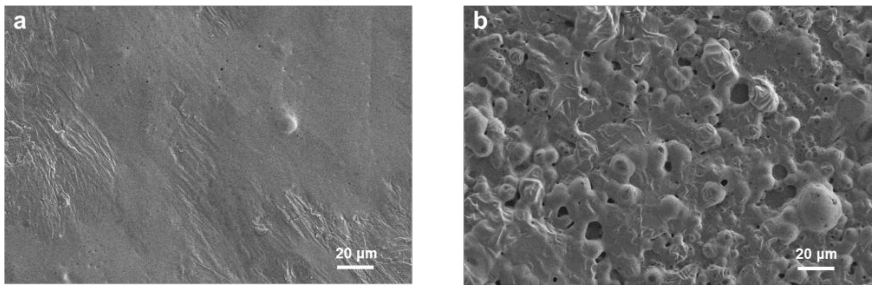

Figure S17. Top-view SEM images of (a) PTV-based SEI and (b) PVC-based SEI after 50 cycles.

Table S1. Elemental composition from XPS measurements at different sputtering times

Sputtering time (s)	Mass concentration (%)					
	PTV-SPE			PVC-SPE		
	C	O	F	C	O	F
0	39.3	34.3	19.3	52.3	40.3	6.0
30	23.5	46.4	27.0	31.3	57.0	9.5
60	19.0	57.5	20.5	23.4	67.6	7.3

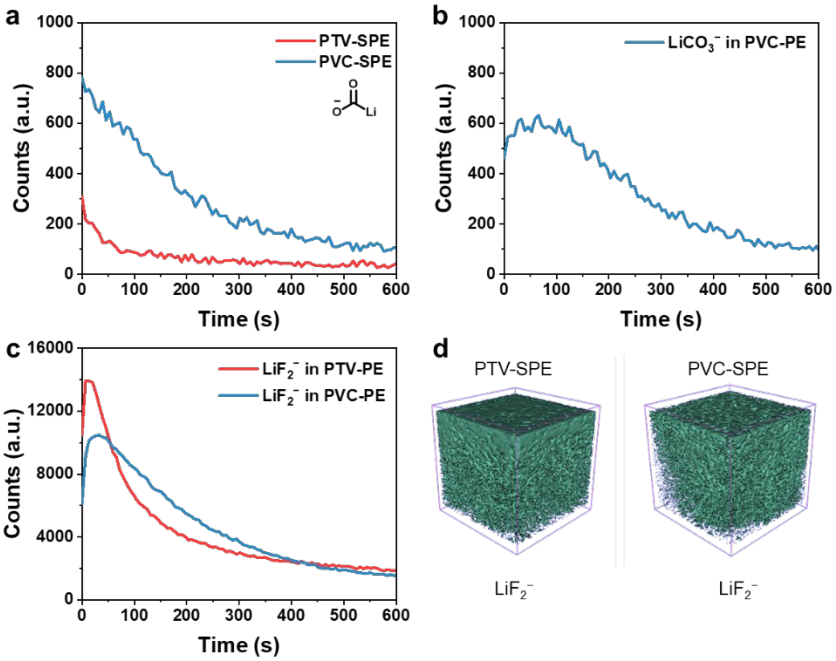

Figure S18. (a) Corresponding TOF-SIMS depth profiles of carbonyl lithium in PTV-based and PVC-based SEIs. (b) Corresponding TOF-SIMS depth profiles of $LiCO_3^-$ in PVC-based SEI. (c) Corresponding TOF-SIMS depth profiles of LiF_2^- in PTV-based and PVC-based SEIs. (d) Corresponding TOF-SIMS 3D mappings of LiF_2^- in PTV-based and PVC-based SEIs.

The counts of degradation byproduct $LiCO_3^-$ in PVC-based SEI (**Figure S18b**) are much higher than that in PTV-based SEI (**Figure 4b**). It suggests that PTV-SPE effectively suppresses the interfacial side reaction. In addition, there is no significant difference in the counts of LiF_2^- in PVC-based SEI and PTV-based SEI (**Figure S18c, d**). This suggests that the reduction in interfacial side reactions is not due to the formation of LiF-rich passivation layers on the surface of LMAs, but rather to the protection of the functional groups of the polycarbonate-based electrolyte by the restricted conformation.

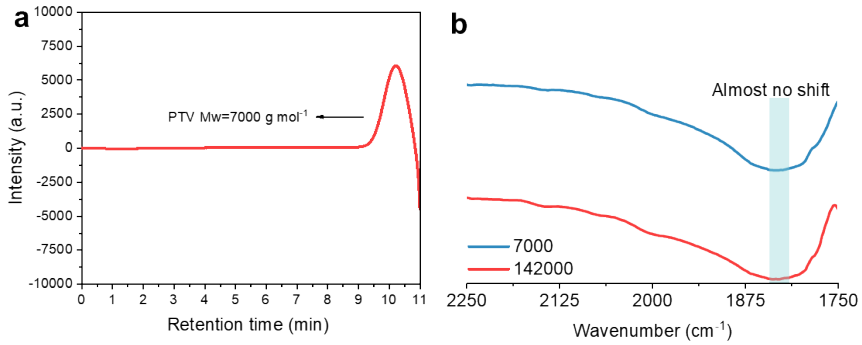

Figure S19. (a) GPC curve of high-concentration PTV-SPE. (b) FTIR spectra of PTV-SPE at different concentrations.

An attempt was made to reduce the time of in situ polymerization to 1 hour to prepare PTV-SPE with low molecular weight (7000 g mol^{-1}). Compared to the high molecular weight PTV-SPE (142000 g mol^{-1}) in this work, low molecular weight PTV-SPE has a higher molecular concentration at a fixed amount of polymer precursor.

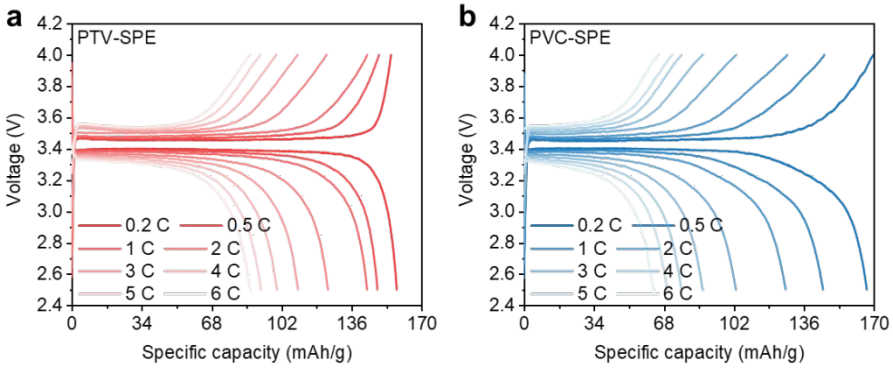

Figure S20. (a) The corresponding charge/discharge profiles at different rates of the PTV-SPE-based LFP/Li cell. (b) The corresponding charge/discharge profiles at different rates of the PVC-SPE-based LFP/Li cell.

References

1. Kresse, G.; Furthmüller, J., Efficient iterative schemes for ab initio total-energy calculations using a plane-wave basis set. *Physical review B* **1996,** *54* (16), 11169.
2. Kresse, G.; Hafner, J., Ab initio molecular-dynamics simulation of the liquid-metal–amorphous-semiconductor transition in germanium. *Physical Review B* **1994,** *49* (20), 14251.
3. Biovia, D. S., Materials studio. *R2 (Dassault Systèmes BIOVIA, San Diego* **2017**.
4. Perdew, J. P.; Wang, Y., Accurate and simple analytic representation of the electron-gas correlation energy. *Physical review B* **1992,** *45* (23), 13244.
5. Grimme, S.; Antony, J.; Ehrlich, S.; Krieg, H., A consistent and accurate ab initio parametrization of density functional dispersion correction (DFT-D) for the 94 elements H-Pu. *The Journal of chemical physics* **2010,** *132* (15), 154104.
6. Nosé, S., A unified formulation of the constant temperature molecular dynamics methods. *The Journal of chemical physics* **1984,** *81* (1), 511-519.
7. Momma, K.; Izumi, F., VESTA: a three-dimensional visualization system for electronic and structural analysis. *Journal of Applied crystallography* **2008,** *41* (3), 653-658.
8. Sun, H., COMPASS: An ab Initio Force-Field Optimized for Condensed-Phase ApplicationsOverview with Details on Alkane and Benzene Compounds. *The Journal of Physical Chemistry B* **1998,** *102* (38), 7338-7364.
9. Sun, H.; Ren, P.; Fried, J. R., The COMPASS force field: parameterization and validation for phosphazenes. *Computational and Theoretical Polymer Science* **1998,** *8* (1), 229-246.
10. Borodin, O.; Olguin, M.; Ganesh, P.; Kent, P. R. C.; Allen, J. L.; Henderson, W. A., Competitive lithium solvation of linear and cyclic carbonates from quantum chemistry. *Physical Chemistry Chemical Physics* **2016,** *18* (1), 164-175.
11. Wan, T. H.; Saccoccio, M.; Chen, C.; Ciucci, F., Influence of the Discretization Methods on the Distribution of Relaxation Times Deconvolution: Implementing Radial Basis Functions with DRTtools. *Electrochimica Acta* **2015,** *184*, 483-499.